Scale effects on the wave-making resistance of ships sailing in shallow water

Zeng, Qingsong; Hekkenberg, Robert; Thill, Cornel; Hopman, Hans

DOI
10.1016/j.oceaneng.2020.107654

Publication date
2020

Document Version
Final published version

Published in
Ocean Engineering

Ocean Engineering 212 (2020) 107654

Contents lists available at ScienceDirect

Ocean Engineering

journal homepage: www.elsevier.com/locate/oceaneng

Scale effects on the wave-making resistance of ships sailing in shallow water

Qingsong Zeng *, Robert Hekkenberg, Cornel Thill, Hans Hopman

Delft University of Technology, 2628CD, Delft, the Netherlands

ARTICLE INFO

Keywords:
Scale effect
Wave-making resistance
Resistance extrapolation
Shallow water

ABSTRACT

The conventional extrapolation of ship resistance from model tests to full scale presumes that the coefficient of wave-making resistance (C_w) depends on the Froude number only. This leads to the assumption that C_w of a ship is identical to C_w of its scaled model. However, this assumption is challenged in shallow water due to viscous effects, which are represented by the Reynolds number (Re). In this study, different scales (different Re) of the Wigley hull and the KCS hull are used to investigate the scale effects on C_w numerically. After verification and validation, systematic computations are performed for both ships and their scaled models in various shallow-water conditions. Based on the results, significantly larger values of C_w are found for the KCS at model scale in very shallow water, suggesting that the conventional extrapolation has to be reconsidered. Additionally, this study reveals the relationship between the changes in frictional resistance coefficient (C_f) and the changes in C_w caused by shallow water, which benefits the prediction of shallow water effects on C_w. Finally, use of a larger ship model, where the Re is also higher, is recommended for resistance tests in shallow water to reduce scale effects on C_w.

1. Introduction

Generally, it is not easy to obtain the resistance of a full-scale ship directly. Conducting ship model tests, therefore, acts as an important technique to predict the full-scale ship resistance. During the tests, the coefficient of wave-making resistance (C_w) is commonly assumed to be a function of Froude number (Fr) only (i.e., independent of viscosity). Thus, C_w remains identical for a ship and its scaled model (ITTC, 2017a). This assumption acts as the basis of resistance extrapolation from model scale to full scale after model tests.

However, researchers have shown that viscosity does have an effect on ship-generated waves. Ship-generated waves will be damped by water viscosity, and Cumberbatch (1965) found that the diverging wave system is damped more heavily than the transverse waves. Calculations conducted by Gotman (2002) showed that a part of the bow wave system is damped by viscosity and will not participate in the interaction with the stern wave system. Likewise, the stern wave system is also damped during its propagation. As a result, C_w achieved in viscous flow is also different from that using potential theory. For instance, small errors might be caused due to the damping if one uses wave-cut analysis (Sharma, 1963) to obtain C_w. As indicated by Stern (1986), the development of the ship's boundary layer is influenced by ship waves. The other way around, ship waves will be affected also by the alternation of the ship's boundary layer. Consequently, similar to the frictional resistance coefficient (C_f), which strongly depends on the ship's boundary layer, C_w will also show scale effects, here being described by the Reynolds number (Re). According to the numerical calculations conducted by Raven et al. (2008), the wave height of ship-generated waves at full scale is larger than that at model scale, indicating that the computed C_w at model scale underestimates a real ship's wave-making resistance. Furthermore, more recently Terziev et al. (2018), using a geosim analysis, argued that C_w does not show clear relationship with neither scale factors nor Re.

Although it was demonstrated that C_w is a function of both Froude number and Reynolds number, a difference in C_w caused by scale effects is generally a small part of the total resistance in deep water. For instance, Raven et al. (2008) computed C_w at both model scale and full scale for the Hamburg Test Case, and the difference between the two values is about 3.3% of the total resistance at full scale. Besides, Terziev et al. (2018) examined the KCS and the change in C_w between model scale and full scale was up to 13.1% of the total resistance at full scale. After using the traditional extrapolation method (ITTC, 2017a), those

* Corresponding author.
E-mail address: zengqingsong2014@163.com (Q. Zeng).

https://doi.org/10.1016/j.oceaneng.2020.107654
Received 28 November 2019; Received in revised form 6 May 2020; Accepted 13 June 2020
Available online 10 July 2020

differences at C_w will not make a big difference (≈5%) in the total resistance at full scale (Zeng, 2019).

Nevertheless, more significant discrepancies can be observed in shallow water. The most obvious difference in ship-generated waves is the change in the angle of the divergent waves (known as Kelvin angle), based on which the subcritical speed regime, critical regime, and supercritical regime are determined (Havelock, 1908). Generally, the value of C_w rises significantly when the depth Froude number, Fr_h, approaches the critical region ($Fr_h \approx 1$) but decreases rapidly immediately after this region. In the supercritical region, the trend that C_w increases with Fr_h is restored. Since most shallow water vessels sail within the subcritical regime, this study will specifically focus on this regime. In this regime, wave properties will be subject to change compared to the deep water case, for instance, ship-generated waves will become faster (Lamb, 1932), higher (Putnam and Johson, 1949), and longer (Mucha et al., 2016). In shallow water, restricted space accelerates the flow around the hull and as a result, the ship's boundary layer becomes thinner, and the wave resistance related to the ship's boundary layer is altered accordingly.

Additionally, the presence of bottom friction can cause a shear current above the fairway floor (Ellingsen, 2014; Li and Ellingsen, 2016) and an extra boundary layer is formed there. This additional boundary layer can induce a shrinkage in the ship's boundary layer due to restricted under-keel clearance. The problem will become even more complicated when these two boundary layers touch each other, and such a situation is expected to vary with Reynolds number. Thus, a hypothesis is proposed that scale effects on C_w will be more significant in shallow water. According to this study, the difference of C_w between model scale and full scale can reach 46.6% of the total resistance of a ship at full scale.

Therefore, the basis of resistance extrapolation, i.e., C_w is insensitive to Re as mentioned above, is challenged. However, to the best of the authors' knowledge, there is no research considering scale effects and shallow water effects on C_w simultaneously. This study is performed to understand the mechanism of scale effects on C_w and to improve the reliability of the ship's resistance extrapolation in shallow water.

CFD (Computational Fluid Dynamics) techniques are applied to obtain C_w separately. Two distinct hull forms, the Wigley hull, and the KCS (KRISO Container Ship) hull, for both of which a large amount of validation data exists, are used in this investigation. Since the purpose is to reveal the mechanism of scale effects on C_w in shallow water, the trim, sinkage, propulsion system, and ship appendices, which are not decisive factors for this mechanism, are not considered for simplification.

This article contains five sections. Section 2 discusses a method for calculating C_w and the setup of numerical cases. Section 3 shows the verification and validation (V&V). Results and analysis are given in Section 4, and conclusions are drawn in Section 5.

2. Method

2.1. The approach for obtaining wave-making resistance numerically

Nominally, the wave-making resistance (R_w) is caused by the energy transferred from the ship hull to the wave system. In deep water, where the effects of viscosity on R_w are minor, wave pattern resistance can be seen as the whole wave-making resistance and can be calculated both numerically through inviscid CFD computations (Raven, 1996) and experimentally through e.g. the wave-cut analysis (Sharma, 1963). However, the accuracy of both methods aforementioned is threatened by the combination of viscosity effects and shallow water effects (Zeng et al., 2019b).

A popular way to obtain R_w separately is conducting two types of resistance test: one with free surface, and another with the free surface suppressed (double-body test). For a bare hull, the coefficient of the total resistance (C_t) can be decomposed into three parts: coefficients of frictional resistance (C_f), viscous pressure resistance (C_{vp}), and wave-making resistance (C_w), which is shown in equation (1):

$$C_t = C_f + C_{vp} + C_w. \tag{1}$$

In equation (1), C_f is calculated by integrating the shear force on the hull surface. In equation (2) below, subscripts "fre" and "dou" are used to represent the results from the scenarios with free surface and double-body tests, respectively. As the $C_{w\_dou} = 0$, the difference of C_t between the two types of situation can be written as:

$$\begin{aligned} &C_{t\_fre} - C_{t\_dou} \\ &= \left(C_{f\_fre} + C_{vp\_fre} + C_w\right) - \left(C_{f\_dou} + C_{vp\_dou}\right) \\ &= \left(1 + k_{fre}\right)C_{f\_fre} - (1 + k_{dou})C_{f\_dou} + C_w. \end{aligned} \tag{2}$$

The symbol k indicates the form factor, which is the ratio between C_{vp} and C_f. Based on equation (2), C_w can be obtained through

$$\begin{aligned} C_w = &\left(C_{t\_fre} - C_{t\_dou}\right) - \\ &\left[\left(1 + k_{fre}\right)C_{f\_fre} - (1 + k_{dou})C_{f\_dou}\right]. \end{aligned} \tag{3}$$

On the right side of equation (3), the variable k_{fre} cannot be achieved directly and precisely through CFD calculations. To solve this problem, two methods to determine C_w exist:

Assumption (i):

$$\left(1 + k_{fre}\right)C_{f\_fre} = (1 + k_{dou})C_{f\_dou} \tag{4}$$

The above assumption indicates that the viscous part of resistance computed with free surface is exactly the same as the total resistance achieved by a double-body calculation. Based on this assumption, equation (3) becomes

$$C_w = C_{t\_fre} - C_{t\_dou} \tag{5}$$

Therefore, C_w is simply the difference between the total forces calculated with and without free surface. This approach is applied frequently especially with the development of CFD techniques, e.g., (Raven et al., 2008).

However, the treatment mentioned above requires the viscous part of the resistance to be identical in both cases. If C_f in one case is higher than another, C_{vp} should be lower to maintain assumption (i). Based on this, C_{vp} appears to be inversely proportional to C_f, which contradicts the conventional understanding of the form factor. To remedy this contradiction, the second approach can be applied.

Assumption (ii):

$$k_{fre} = k_{dou} \tag{6}$$

Equation (6) assumes the form factor (k) remains the same for both cases with free surface and its corresponding double-body test. Since most ships in shallow water navigate at a relatively low speed, waves generated by the ship hull generally have a small wave height, which makes the pressure distribution on the hull, as well as the wetted surface, almost identical between the cases with and without free surface, except for very limited areas near the free surface. In addition, for the two ships (i.e., the Wigley hull and the KCS, as will be discussed in Section 2.2.1) that will be used in this study, the streamlined stern helps prevent wave-induced flow separation at the aft, by which the pressure field behind the stern remains similar for both conditions. Thus, the forces on the hull are similar for both cases with and without free surface. Therefore, since C_f and C_{vp} are computed based on the same wetted surface, the form factor can thus be seen as identical with minor errors for both cases, i.e., C_{vp} is proportional to C_f, which underpins assumption (ii) mentioned above. Consequently, equation (3) becomes

$$C_w = \left(C_{t\_fre} - C_{t\_dou}\right) - (1 + k_{dou})\left(C_{f\_fre} - C_{f\_dou}\right) \tag{7}$$

Assumption (ii) will be implemented in this study. All coefficients on the right side of equation (7) can be obtained through CFD

computations, which makes it possible to determine C_w separately and numerically in shallow water.

2.2. Setup of cases

2.2.1. Ship information

In this study, the ship/model scale, which is expressed by the Reynolds number (Re), is proposed as an additional influencing factor on wave-making resistance in shallow water, i.e., $C_w = \mathrm{f}(Fr, Re)$. According to the research of Zeng et al. (2019a), a ship with a higher block coefficient (C_B, which represents the fullness of a ship) tends to show more obvious scale effects on the viscous part of the resistance in shallow water. Therefore, the scale effects on C_w depend on the ship's fullness, and two ships with a distinctly different fullness, the Wigley hull, and the KCS are selected since a large amount of validating data is available. The underwater part for each ship is shown in Fig. 1.

The Wigley hull is a representative of slender ships. It has no flat bottom and $C_B = 0.445$. The surface of the Wigley hull can be defined precisely by equation (8) (e.g., Kajitani et al. (1983)):

$$y = \frac{B}{L}\left(1 - \left(\frac{2x}{L}\right)^2\right)\left(1 - \left(\frac{z}{T}\right)^2\right) \tag{8}$$

where B is the ship's beam, L the ship's length (due to the symmetry of the Wigley hull, the length between perpendiculars L_{pp} is identical to L), and x, y, z are the coordinates in a Cartesian coordinate system. x is positive in the navigation direction, y is positive to port, and z is positive upward. This coordinate system is also valid for the KCS except for the position of the origin. For the Wigley hull, the origin is the intersection of the midsection, the symmetric plane, and the design waterline plane. For the KCS, the origin is the intersection of the aft perpendicular and the zero waterline plane.

Compared to the Wigley hull, the KCS hull has a much fuller shape ($C_B = 0.651$) and a large area of the flat bottom (see e.g., Kim et al. (2001) for more details). More information about these two ships at full scale is listed in Table 1. For the "full-scale" Wigley hull, the length and the design velocity are set deliberately to 75 m and 5.196 m/s (corresponding to 18.705 km/h for an inland vessel), respectively, which are representative values for typical inland ships. The velocity of the full-scale KCS is 7.893 m/s, at which the depth Froude number (Fr_h) is the same as the Wigley hull, thus enabling a clear comparison. Specific values of velocities are determined based on an easily interpretable value of Reynolds number (Re), i.e., $\lg(Re) = 8.50$ for the Wigley hull and $\lg(Re) = 9.20$ for the KCS at full scale.

To study scale effects on wave-making resistance, different scale factors that lead to a length of ship models within 1.5 m–15 m are selected, which covers the typical range of the model length used by most towing tanks in the world. Again, specific values for the scale factor are chosen to ensure the Wigley hull and the KCS hull have the same

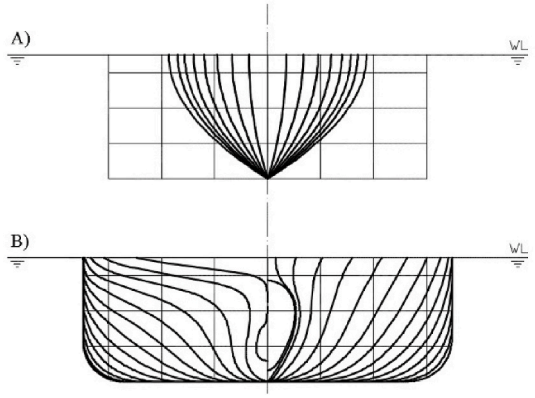

Fig. 1. Lines plan for the underwater part of A) the Wigley hull and B) the KCS.

Table 1
Parameters of the Wigley hull and the KCS (Kajitani et al., 1983; Kim et al., 2001).

	Note	Unit	Wigley hull	KCS
L_{pp}	Length between perpendiculars	m	75.000	230.000
B	Beam	m	7.500	32.200
T	Draft	m	4.680	10.800
C_B	Block coefficient	–	0.445	0.651
S	Wetted surface	m^2	837.000	9545.593
V	Designed velocity	m/s	5.196	7.893

value of Re, as shown in Table 2. It should be pointed out that the Re starts at $\lg(Re) = 6.0$. Although a laminar boundary layer would cover half of a flat plate at $\lg(Re) = 6.0$ based on the research of Eça and Hoekstra (2008), it is found that for the ship hulls in this study, about 90% (instead of 50%) of the hull will be covered with a turbulent boundary layer due to the initial turbulence intensity and the 3D hull effects. Thus, the influence of the laminar flow at $\lg(Re) = 6.0$ can be considered as negligible in the computation of ship resistance. For each selected ship, the Froude number, Fr, is kept as constant. A commonly used non-dimensional factor y^+, which represents how far the first grid point is located from the wall, for each case is also shown in Table 2. The value of y^+ is estimated prior to the calculations, as will be discussed in detail in Section 3.1.1.

2.2.2. Waterway dimensions

Shallow water conditions are realized by adjusting the vertical position of the waterway floor, which can be described by the water-depth/ship-draft ratio (h/T). Four shallow-water scenarios with h/T equals 2.0, 1.5, 1.3, and 1.2 are applied, and one deep water case ($h/T \approx 15$) is included for comparison, as shown in Table 3. Combined with Table 2, there will be 70 cases in total in this study.

In this study, the waterway is assumed to be only limited in water depth. Thus, the lateral boundary should be far enough away from the ship to avoid blockage effects, regardless of the boundary condition assigned to it. According to ITTC (2017), and also the CFD computations performed by Zeng et al. (2019a), the blockage factor (m), which is the ratio between the area of ship's midsection and the area of the wetted waterway section, should be less than 3% to eliminate blockage effects. Therefore, the water-width/ship-length ratio (W/L_{pp}) is adjusted to meet the requirement, as shown also in Table 3. For comparison purposes, the depth Froude numbers (Fr_h) for the Wigley hull and the KCS are designed to be identical for each h/T.

Fr_h higher than 0.7000 is rarely found for vessels sailing in shallow water and is therefore not discussed.

2.2.3. Numerical settings

2.2.3.1. Computational domain and boundary conditions. Due to the symmetry of the ship, half of the domain is used in the computations. The inlet boundary is 1 L_{pp} in front of the ship, and the outlet boundary is 3 L_{pp} behind the ship. For cases with free surface, the top boundary is located 0.5 L_{pp} above the designed waterline plane. The position of the bottom varies with h/T. Sketches for the computational domain are shown in Fig. 2.

Boundary conditions for both cases are also shown in Fig. 2. The ship hull is a non-slip wall and fixed in the domain. Water comes from the inlet boundary with the same velocity as the ship's design speed. The bottom boundary is a "moving wall", which is non-slip and moving at the same speed as the incident flow.

For computations without free surface, the Dirichlet boundary condition is applied for the "velocity inlet" boundary, where the value of input velocity is given before simulations; the Neumann boundary condition is used for the "outflow" boundary, where the diffusion flux for all flow variables is zero in the direction normal to the outlet plane.

Table 2
Reynolds number (Re), scale factor, Froude number (Fr), length, velocities (V) and the initial mean wall $y+$ for the Wigley hull and the KCS.

lg(Re)	Wigley						KCS					
	Scale	Fr	Length(m)	V(m/s)	V (km/h)	Wall $y+$	Scale	Fr	Length(m)	V (m/s)	V (km/h)	Wall $y+$
6.0	48.90	0.1915	1.534	0.743	2.675	4	136.50	0.1662	1.685	0.676	2.432	2
6.3	30.00	0.1915	2.500	0.949	3.415	4	84.40	0.1662	2.725	0.859	3.093	2
6.5	22.70	0.1915	3.304	1.091	3.926	4	63.35	0.1662	3.631	0.992	3.57	4
6.8	14.32	0.1915	5.237	1.373	4.943	30	40.00	0.1662	5.750	1.248	4.493	30
7.0	10.54	0.1915	7.116	1.600	5.761	30	31.60	0.1662	7.278	1.404	5.055	30
7.4	5.71	0.1915	13.135	2.174	7.828	50	16.00	0.1662	14.375	1.973	7.104	50
8.5	1.00	0.1915	75.000	5.196	18.705	100	–	–	–	–	–	–
9.2	–	–	–	–	–	–	1.00	0.1662	230.000	7.893	28.414	400

Table 3
Water-depth/ship-draft ratio (h/T), blockage factor (m), and depth Froude number (Fr_h) for the Wigley hull and the KCS (W is the width of waterway, L_{pp} is ship length between perpendiculars).

No.	Wigley				KCS			
	h/T	m	W/L_{pp}	Fr_h	h/T	m	W/L_{pp}	Fr_h
1	15.06	0.2%	3.0	0.198	15.00	0.3%	3.0	0.198
2	2.00	1.7%	3.0	0.542	2.00	1.8%	4.0	0.542
3	1.50	2.2%	3.0	0.626	1.50	2.3%	4.0	0.626
4	1.30	2.6%	3.0	0.673	1.30	2.7%	4.0	0.673
5	1.20	2.8%	3.0	0.700	1.20	2.9%	4.0	0.700

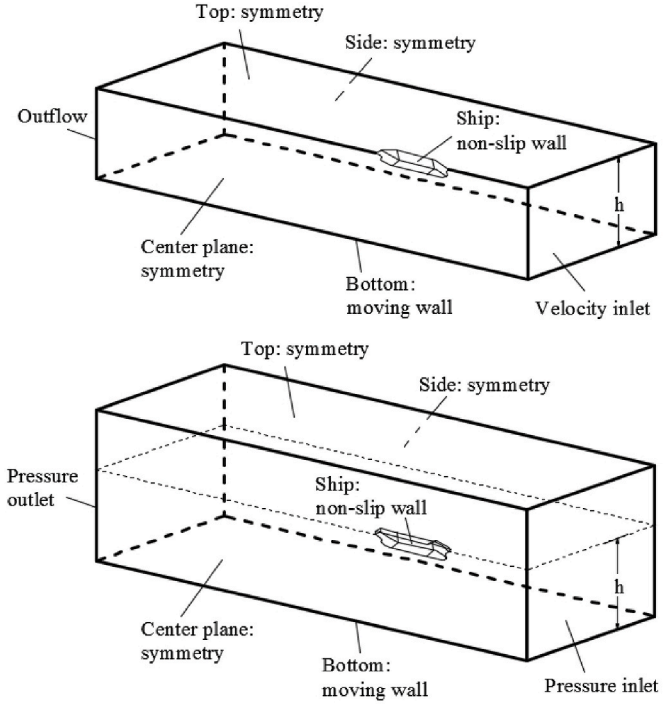

Fig. 2. Computation domain and boundary conditions for cases without free surface (top) and with free surface (bottom).

For computations with free surface, the VOF (Volume of Fluid) technique and the open channel boundary condition are used. To adjust to the open channel method, "Pressure inlet" and "pressure outlet" are applied for the inlet and outlet boundary, respectively.

2.2.3.2. Mesh and solver. For all cases in this study, a hexahedral mesh is generated through ICEM (version 18.1). The underwater part of the mesh is identical for the condition with free surface and its corresponding double-body case in terms of C_w calculation. The grids close to the hull and the waterway floor are refined in order to properly capture the complexity of the flow. An example is shown in Fig. 3 for the KCS with $h/T = 1.2$. The thickness of the first layer of the mesh adjacent to the hull depends on the choice of y^+, which will be discussed in detail in Section 3.1 "Verification".

All CFD computations are run on a commercial solver ANSYS Fluent (version 18.1). The turbulence is resolved approximately by solving the Reynolds-averaged Navier–Stokes (RANS) equations with the application of the SST k-ω model. The steady pressure-based solver is used. The pressure and the velocity are calculated in a coupled manner. The discretization methods for gradient and pressure are Least Squares Cell-Based and PRESTO! (PREssure staggering Option), respectively. The discretization method is second-order upwind for momentum, turbulent kinetic energy, and specific dissipation rate.

3. Verification and validation

In this section, the code Fluent is firstly verified by evaluating the uncertainties of spatial discretization, the uncertainties of temporal discretization, and the effects of y^+ on wave-making resistance. Afterward, the code is validated by computing the wave profile close to the ship hull and the total resistance.

3.1. Verification

3.1.1. Spatial discretization uncertainty

In the solver Fluent, the velocity and the pressure in the flow field are not solved continuously. Their values are calculated in the center of the grid cells and the interpolation method is utilized if no computed point exists. Thus, to reduce the numerical errors caused by mesh to an acceptable level, the uncertainties of the spatial discretization are evaluated.

This verification follows the method proposed by Eça and Hoekstra (2014), which is shown as follows:

$$S_{RE}\left(\varphi_0, \beta, p\right) = \sqrt{\sum_{i=1}^{N}\left(\varphi_i - (\varphi_0 + \beta\alpha_i^p)\right)^2}, \tag{9}$$

where φ_i is the key variable to be evaluated, which will be the frictional resistance coefficient (C_f) and the total resistance coefficient (C_t). φ_0, β, p

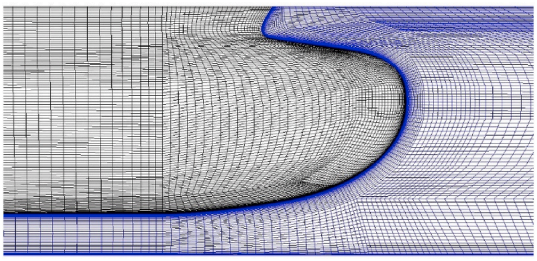

Fig. 3. Part of the mesh showing the grids close to the bulbous bow of the KCS with $h/T = 1.2$.

are constants derived from a fitting curve of φ_i. The value of p indicates the order of accuracy. The uncertainty can be obtained through

$$U(\varphi_i) = F_s|(\varphi_i - \varphi_0)| + S_D + |\varphi_i - (\varphi_0 + \beta\alpha_i^p)|, \tag{10}$$

where S_D is the standard deviation. $F_s = 1.25$ if $0.5 \leq p < 2.1$, otherwise, $F_s = 3$. In order to use this method, at least four sets of mesh are required.

In the experiments conducted by Kim et al. (2001), a 1/31.6 ship model of the KCS is applied. The Froude number is 0.26 and is also used in this verification. The refinement factor, r, in each direction is 1.25, and four sets of mesh are implemented. In Table 4, the number of grid cells, the results of C_f and C_t, and the number of grid nodes per wavelength, N, are listed. In this verification, a constant value of $y^+(= 50)$ is used. It was determined prior to the simulations through equation (11):

$$\begin{aligned} y^+ &= \frac{u^* y}{\upsilon} \\ u^* &= \sqrt{\frac{\tau}{\rho}} \\ \tau &= C_{f57}\cdot\frac{1}{2}\rho V^2 \end{aligned} \tag{11}$$

where u^* is the friction velocity, y is the exact distance (m) of the first grid point from the wall, υ water kinematic viscosity, τ the shear stress, ρ water density, C_{f57} the frictional resistance coefficient (calculated by the ITTC (1957) line) and V the water velocity.

Based on Table 4, the method of Eça and Hoekstra (2014) mentioned above is applied to calculate the uncertainties of C_f and C_t. Generally, the geometrical similarity should be maintained in the complete computational field. Based on this assumption, the distance between the first grid point and the wall (described by y^+) varies in those grid sets. However, different values of y^+ also determine whether a wall function is applied or not, and the results of C_f will be affected accordingly. Consequently, scatters might be caused leading to an unprecise asymptotic region. Therefore, a constant wall y^+ is applied, and the grid distribution in other places is geometrically similar. The spatial discretization errors and uncertainties of C_f and C_t of the 1/31.6 KCS for the finest mesh (mesh set No. 1) are calculated and shown in Table 5.

Table 5 shows that the uncertainties of both C_f and C_t caused by spatial discretization are less than 2%, which is acceptable for a numerical calculation. Therefore, the finest grid set is selected in the subsequent sections.

However, the spatial convergence study is specifically for the 1/31.6 scaled KCS at $Fr = 0.26$ and $y^+ = 50$. As mentioned in Section 2.2.2, there will be 70 cases in total. It is not practical to perform such verification for all cases. Therefore, a more general rule, which is the number of nodes per wavelength, applicable to all other cases, is discussed.

Since the density of grid points per wave period determines the accuracy of wave profile and thus influences the wave-making resistance, the number of nodes per wave height and/or per wavelength is a good candidate to act as a general key factor for spatial convergence study.

In this subsection, the number of grid points over the height of the wave is about 10, and the aspect ratio of the cells near the free surface is at the magnitude of 10. This setting was proven to be suitable, and increasing the number of grid points in one wave height will make a minor contribution to the sharpness of the wave profile (Javanmardi, 2015). Therefore, this study will focus on the choice of the number of grid points per wavelength.

Table 4
Parameters and resistance coefficients of each set of mesh for the 1/31.6 KCS at $Fr = 0.26$ ($y^+ = 50$).

No.	Cells (million)	C_f ($\times 10^3$)	C_t ($\times 10^3$)	N
1	8.91	2.8084	3.5665	104
2	4.56	2.8051	3.5753	87
3	2.34	2.8006	3.5968	70
4	1.20	2.7932	3.6342	56

Table 5
The spatial discretization uncertainties of C_f and C_t for the 1/31.6 KCS at $Fr = 0.26$ ($y^+ = 50$).

Key variable	C_f	C_t
φ_0	2.812E-03	3.555E-03
α	−4.482E-06	1.181E-05
p	2.178	2.848
S_D	1.166E-06	2.876E-06
Error	1.572E-05	4.882E-05
Uncertainty	0.56%	1.74%

Linear wave theory (Airy, 1841) is applied to predict the number of wavelengths along with the ship hull. Based on this theory, the number of ship-generated waves within a ship length distance (n) is a function of Froude number (Fr):

$$n = \frac{1}{2\pi Fr^2}. \tag{12}$$

Equation (12) makes it possible to estimate the wavelength and thus the number of grid points per wavelength (N) before numerical calculations. In Table 4, the value of N for each mesh set is shown in the last column. A wave-cut at $y = 2B$ is depicted in Fig. 4 for each case in the range of $x = -2.5\ L_{pp} \sim 1.5\ L_{pp}$.

Based on Fig. 4, it can be found that.

- The wave profile generated with $N = 56$ has a relatively large deviation compared to $N = 104$ (where the wave profile is assumed to be the most accurate). Therefore, $N = 56$ is not considered for the area close to the hull where a high accuracy of the wave profile is required;
- In the range of $N = 70$–104, the sharpness of the wave profile increases with a refinement of the mesh, but the differences are becoming smaller, which means the refinement of the mesh only makes small contributions to the wave sharpness.

Therefore, to balance the accuracy and computation costs, $N \geq 56$ is guaranteed for the far field, and $N \geq 70$ is guaranteed for the area close to the ship hull, by which the accuracy of the calculated resistance and the wave sharpness close to the hull are assured. The number of cells finally applied for each case in deep water are shown in Table 6.

The number of cells for each shallow water case is not listed, since the number of cells decreas corresponding to the value of under-keel clearance and other parts remain the same as the deep water case.

3.1.2. Temporal discretization uncertainty

In addition to the verification of spatial discretization, an appropriate time step should be selected to guarantee a good convergence. The basic requirement in a CFD computation is that the Courant number ($C = V \cdot \Delta t/\Delta x$, where V is the flow velocity, Δt the time step applied, and Δx the length interval) should be less than one. In (ITTC, 2017b), a more rigorous requirement, $\Delta t < 0.01L/U$, is suggested, where L is ship length and U ship speed.

During the simulations, a steady solver is used but the "Automatic Pseudo Transient Time Step" is enabled. In Fluent, Δt is selected automatically (ANSYS, 2017) by

$$\Delta t = \min\left(\Delta t_u, \Delta t_p, \Delta t_g, \Delta t_{rot}, \Delta t_{compress}\right), \tag{13}$$

where Δt_u is the convective time scale, Δt_p the dynamic time scale, Δt_g the gravitational time scale, Δt_{rot} the rotational time scale, and $\Delta t_{compress}$ the compressible time scale. Details can be found in ANSYS (2017). The physical time step is controlled by the Time Scale Factor. In this temporal verification, case No.4 in Table 4 is used. Again, the refinement factor is 1.25, and four values of the time step are applied. The

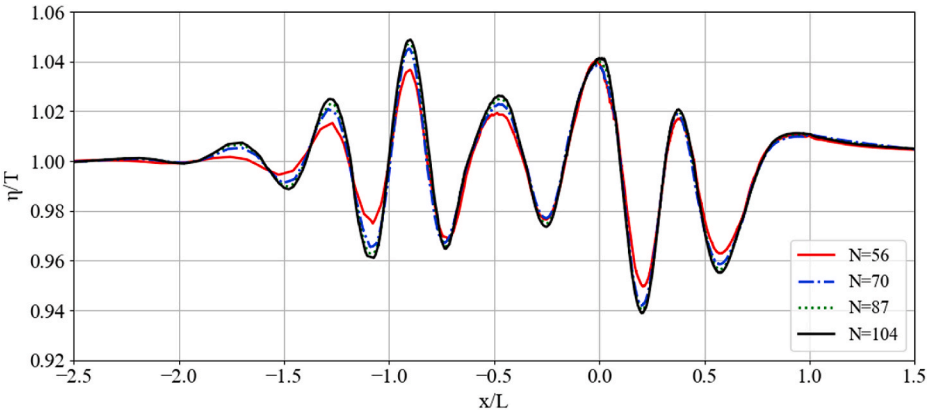

Fig. 4. The wave cut at $y = 2B$ for different number of nodes per wavelength (N) in the range of $x = -2.5\ L_{pp} \sim 1.5\ L_{pp}$ (η: free surface elevation, $Fr = 0.26$; the 1/31.6 scaled KCS locates at $x = 0$–$1.0\ L_{pp}$ with the bow at $1.0\ L_{pp}$).

Table 6
The number of cells for each case in deep water (Unit: million).

lg(*Re*)	Wigley		KCS	
	Free surface	Double body	Free surface	Double body
6.0	4.89	2.76	9.10	5.31
6.3	5.06	2.76	9.29	5.44
6.5	5.62	2.91	9.10	5.44
6.8	5.97	2.91	8.91	5.18
7.0	7.06	3.06	8.91	5.31
7.4	7.41	3.56	9.10	5.31
8.5	9.39	4.49	–	–
9.2	–	–	9.29	5.57

uncertainties caused by temporal discretization for the case Δt_2 are shown in Table 7.

In Table 7, although the uncertainties are calculated for Δt_2 (not the smallest time step), the uncertainties for both C_f and C_t are very small (<0.02%). Therefore, Δt_2 is used for all subsequent calculations to balance computing accuracy and time.

3.1.3. The choice of y^+

The y^+ dependency of the wave-making resistance is studied in this subsection. According to ITTC (2017b), $y^+ \leq 1$ is recommended when a near-wall turbulence model is used, and $30 < y^+ < 100$ is recommended when a wall function is used. However, those suggested regions only cover a limited range of y^+. Also, the value of y^+ is not a constant along with a ship hull in the numerical results, which will make the near-wall meshing work extremely complicated if the rules mentioned above are met rigorously. To solve this problem, many industrial CFD codes apply the so-called "y^+-insensitive" wall treatments by using blending functions for the buffer region and the fully-turbulent outer region, e.g., the Menter-Lechner treatment is applied for ω-equation models in Fluent (ANSYS, 2017).

In principle, the choice of y^+ will influence the results for shear stress on a non-slip wall, and the frictional resistance can be affected by y^+. In this study, since wave-making resistance is assumed to also depend on Reynolds number, the choice of y^+ may also make a difference in the wave resistance. This subsection is established to test whether the wave-making resistance is invariant with y^+ if the SST k-ω model is used in Fluent.

According to the research of Zeng et al. (2019a), the resistance of the KCS is more sensitive to water depth than the Wigley hull. Therefore, the case of the KCS in shallow water ($h/T = 1.2$) is selected for this y^+ test. About the choice of Re, lg(Re) = 7.4 is used since the mesh quality is generally not acceptable by the solver when $y^+ \geq 150$ for lg(Re) < 7.4, and an excessively large number of cells is obtained when $y^+ \leq 8$ for lg (Re) > 7.4.

The values of y^+ used in this study are shown in Table 8. A deep-water ($h/T = 15.0$) case is analysed for comparison. The selected y^+ varies from 1 to 400, which spreads over all the regions in the inner and outer boundary layer. Due to a limitation on available physical memory, cases with more than 12 million grid points are not performed, which are marked by "-" in Table 8.

For the case with $y^+ = 400$ the first computed point is in the outer layer, which is included to study the usability of the code in this specific region. The results of C_w using the method proposed in Section 2.1 are shown in Fig. 5. CFD results of C_f and the results calculated by ITTC (1957) and Katsui et al. (2005) are also shown for demonstration.

From Fig. 5, it can be derived that.

Table 7
Temporal discretization errors and uncertainties of C_f and C_t for the 1/31.6 KCS at $Fr = 0.26$ ($y^+ = 50$).

Key variable	C_f	C_t
0.01 L/U (s)	0.0331	0.0331
Δt_1 (s)	0.0169	0.0169
Δt_2 (s)	0.0212	0.0212
Δt_3 (s)	0.0265	0.0265
Δt_4 (s)	0.0317	0.0317
φ_0	2.792E-03	3.643E-03
α	3.373E-08	−5.794E-07
p	5.500	4.144
S_D	3.445E-15	1.603E-12
Error	1.880E-07	3.638E-06
Uncertainty	0.001%	0.018%

Table 8
The selected values of y^+ for deep ($h/T = 15.0$) and shallow water ($h/T = 1.2$) (the cases marked with "-" are not performed due to the limited physical memory).

y^+	Deep water		$h/T = 1.2$	
	Double-body	Free surface	Double-body	Free surface
1	+	–	+	–
2	+	–	+	–
4	+	+	+	+
8	+	+	+	+
16	+	+	+	+
30	+	+	+	+
50	+	+	+	+
75	+	+	+	+
100	+	+	+	+
150	+	+	+	+
200	+	+	+	+
400	+	+	+	+

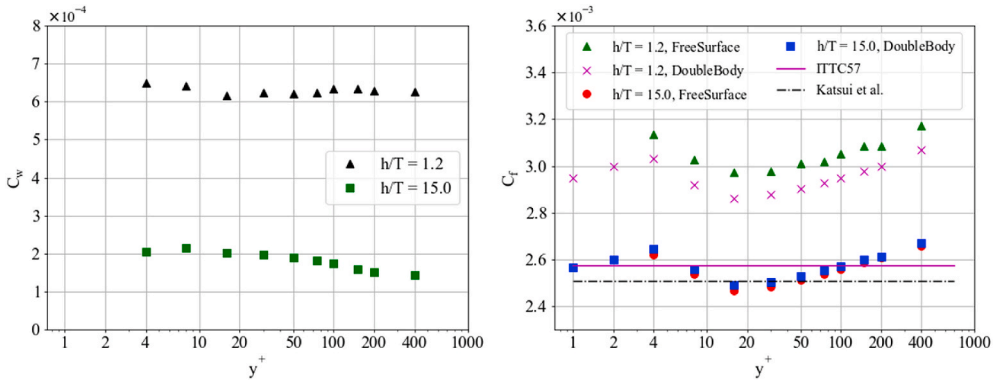

Fig. 5. CFD results of the coefficient of wave-making resistance (C_w) (left) and the coefficient of frictional resistance (C_f) (right) against y^+ in deep and shallow water.

- The fluctuation of C_w at $h/T = 15$ is about ±20% compared to its average; C_w at $h/T = 1.2$ varies within ±2% compared to the C_w average. The absolute fluctuations at $h/T = 15$ and at $h/T = 1.2$ are at the same order of magnitude despite their distinctly different relative values. However, the average C_w at $h/T = 1.2$ is 242% higher than $h/T = 15$, which is one order of magnitude larger than the individual fluctuations. It means that shallow water effect on C_w of the KCS is one order of magnitude larger than the influence of y^+;
- For C_f at $h/T = 15$, a different choice of y^+ will cause ±3% differences in C_f compared to its average value for both conditions with and without free surface. Besides, for the same choice of y^+, whether the free surface is considered will hardly change C_f (<1%);
- For C_f at $h/T = 1.2$, similar to the deep-water condition, the choice of y^+ leads to ±3% difference on C_f for both free surface and double-body conditions. Nevertheless, for the same y^+ with and without free surface, the difference can reach up to 6%, which is much larger than in the deep-water condition. It should be mentioned that the influence of this discrepancy can be eliminated using equation (7) to calculate C_w;
- In deep-water condition, the values of C_f are close to the lines given by ITTC57 and Katsui et al. This phenomenon qualitatively proves the reliability of C_f computation since none of these two lines can be seen as completely accurate for the prediction of ship's friction;

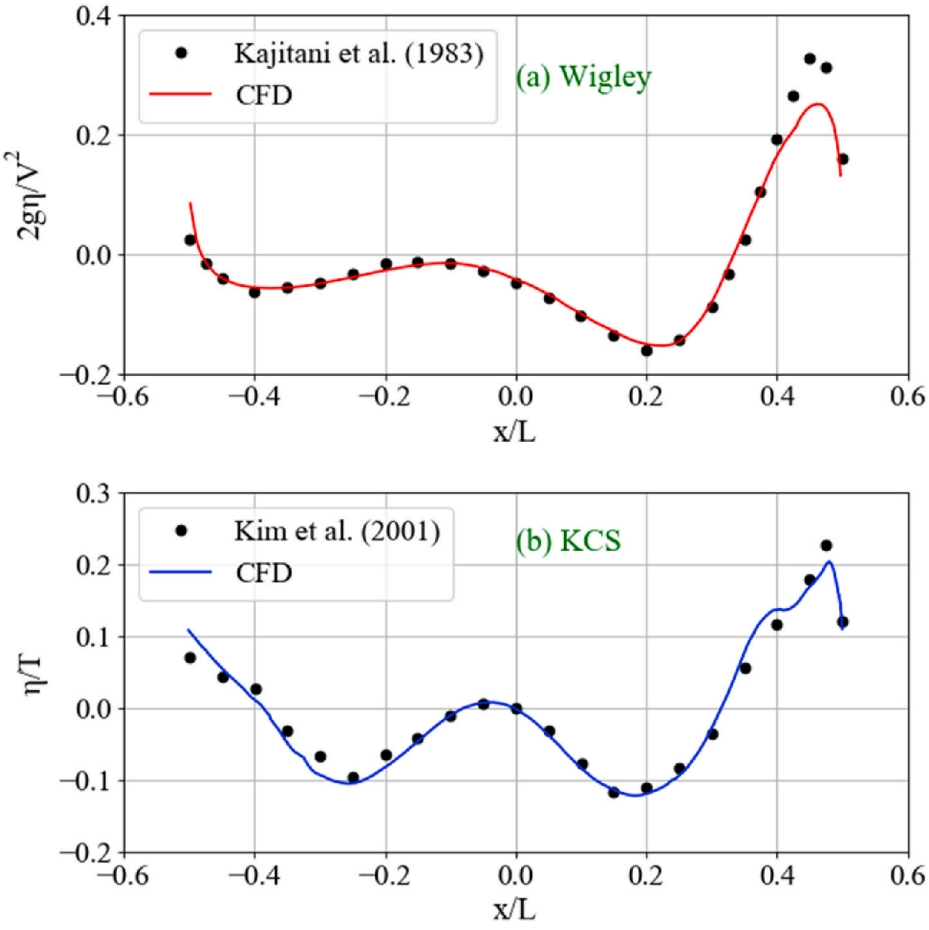

Fig. 6. The validation of the free surface elevation along with the Wigley hull (top figure, $Fr = 0.316$) and the KCS (bottom figure, $Fr = 0.26$).

- When $y^+ = 400$, the code can still provide reasonable results for C_f and C_w, which means that placing the first grid point in the outer layer can be practically acceptable based on this code.

Therefore, since shallow water effects on C_w of the KCS is one order larger than the influence of y^+, C_w is seen as independent of y^+ in this study. For each specific case, the value of y^+ for each Reynolds number is already listed in Table 2. For a computation with free surface and its corresponding double-body calculation, the same y^+ is applied.

3.2. Validation

The CFD code applied in this study is validated using publishedmodel tests. The key variables are the free surface elevation along with the hull and the total resistance coefficient (C_t). For the Wigley hull, a test with a 2.5 m long Wigley model performed by Kajitani et al. (1983) is applied, and a CFD case in deep water with $N = 80$ close to the hull, $Fr = 0.316$, and $y^+ = 4$ is used. For the KCS, an experiment with a 1/31.6 model conducted by Kim et al. (2001) is applied, and a CFD case with $N = 104$ close to the hull, $Fr = 0.26$, and $y^+ = 50$ is used.

In Fig. 6, a comparison is made for the free surface elevation (η) generated by the CFD computation and the experimental data. It can be seen that for both the Wigley hull and the KCS, the CFD results have a good agreement with the experiments. Small differences are observed in a limited area close to the bow and stern, which might be caused by a high pressure gradient combined with a relatively coarse mesh. A refinement of the mesh can help to improve the results. However, the error is located in a small area, and its influence on the total resistance is not significant, which will be discussed later.

For the Wigley hull, the value of C_t computed by CFD code is 5.286×10^{-3}. It is 2.65% larger than the test result given by Kajitani et al. ($C_t = 5.149 \times 10^{-3}$). For the KCS, the computed C_t is 3.447×10^{-3} which is 3.10% smaller than the test result (3.557×10^{-3}). Errors in both cases are considered acceptable for a numerical calculation.

As a supplement, the validation standard uncertainty (u_{val}) can be calculated by equation (14) following the method proposed by ASME PTC Committee (2009):

$$u_{val} = \sqrt{u_{num}^2 + u_{input}^2 + u_D^2} \tag{14}$$

where u_{num} is the numerical uncertainty derived from the verification, u_{input} the input uncertainty, and u_D the standard uncertainty of the experimental data.

In Section 3.1, since the value of u_{num} for the KCS was discussed, it is possible to calculate the u_{val} for the KCS. As the spatial discretization uncertainty is two orders higher than the temporal discretization uncertainty, the former is used to represent the u_{num}. In addition, since the input parameters, such as the velocity, free surface position, etc., are exactly the same as in the real world, the value of u_{input} can be seen as negligible. For the uncertainty of experiments (u_D) of the total resistance, a value of 1% was provided for the KCS (Kim et al., 2001). Consequently, based on equation (14), the validation standard uncertainty (u_{val}) for the KCS is derived as 2.01%, which is seen as acceptable for a simulation.

Therefore, it is concluded that the selected code with the settings used in this study is able to generate acceptable results of both wave profile and ship resistance. It will be used for the systematic calculations in the following section.

4. Results and discussion

4.1. CFD results and analysis

CFD results of C_w, calculated following the method mentioned in Section 2.1, at different scales of the Wigley hull and the KCS (listed in Table 2) with various depth Froude number (Fr_h, listed in Table 3) are shown in Fig. 7.

Based on Fig. 7, scale effects on wave-making resistance for both ships are analysed as follows:

- When $Fr_h \leq 0.5422$, the wave resistance coefficient (C_w) can still be seen as independent of the Reynolds number for both ships. The traditional extrapolation, in which C_w is only a function of Froude number, is still reliable;
- When $Fr_h = 0.6261$, C_w of the KCS at model scale begins to show significantly larger values than full scale, e.g., C_w of the KCS increases by 44% at $\lg(Re) = 6.0$ compared to $\lg(Re) = 9.2$. However, C_w of the Wigley hull is insensitive to Reynolds number (Re) at this Fr_h, which indicates that the ship form plays an important role in the scale dependency (or Re dependency) of C_w;
- When $Fr_h \geq 0.6725$, more significant effects of Re on C_w are observed for the KCS, e.g., for $Fr_h = 0.7000$, C_w of the KCS increases by 218.6% at $\lg(Re) = 6.0$ compared to $\lg(Re) = 9.2$, The increment of C_w (1.446×10^{-3}) at $\lg(Re) = 6.0$ even reaches the same order of magnitude as C_f (1.823×10^{-3}) at $\lg(Re) = 9.2$. Such a change of C_w is 14.9% of C_t at the model scale and takes approximately 46.6% of C_t at full scale. For slender ships such as the Wigley hull, however, much smaller increments (27%) of C_w can be found at low Re range and will also not cause large errors on C_t even for $Fr_h \geq 0.6725$;
- In general, scale effects on C_w are decreasing with an increasing Reynolds number. This is in line with the common sense that the effect of viscosity on ship resistance becomes smaller when the Reynolds number is larger.

Therefore, the traditional assumption that the wave-making resistance coefficient is independent of ship/model scales is still valid at $Fr_h \leq 0.5422$ for both ships and with all values of Fr_h for slender ships like the Wigley hull. In these conditions, the conventional extrapolation of ship resistance from model tests can be applied in shallow water without any corrections. However, the extrapolation should be reevaluated when $0.5422 < Fr_h \leq 0.7000$ for fuller ships like the KCS, since its Re dependency of C_w is confirmed in this study.

4.2. Discussion

According to the analysis in Section 4.1, when the Reynolds number is relatively low and the ship is relatively full (the KCS), an obvious increase at C_w is found in shallow water. Coincidently, the frictional resistance coefficient (C_f) also increases compared to full-scale ships in similar conditions Zeng et al. (2019a). This phenomenon provides a hint that the changes in C_w in shallow water have a strong relationship with the changes in C_f.

For the model scale, the thickness of the boundary layer on the ship's bottom can reach the same magnitude as the under-keel clearance (ukc). However, this generally does not apply to full-scale ships. An example is given in Fig. 8. In this figure, contours of velocity for part of the space under the KCS are shown for $\lg(Re) = 6.0$ and $\lg(Re) = 9.2$.

As is depicted in Fig. 8, the boundary layer on the ship's bottom at $\lg(Re) = 6.0$ is much more obvious compared to $\lg(Re) = 9.2$. For $\lg(Re) = 6.0$, the boundary layer grows faster from the bow to the stern, making the flow velocity and also pressure distribution in the under-keel space completely different from the scenario of $\lg(Re) = 9.2$. Therefore, the similarity of flow structures at model scale and full scale cannot be guaranteed in shallow water. This is the physical explanation for why yet unconsidered scale effects need to be considered in shallow water.

Since the flow field around the hull is altered by shallow water and viscosity, the shear stress (C_f related) and the pressure (C_w related) on the ship hull are also changed accordingly and simultaneously. Thus, as mentioned before, a relationship between the changes at C_w and the changes at C_f in shallow water is expected. If this relationship is established, performing computations with free surface only can provide enough information to estimate possible scale effects on C_w. In this case,

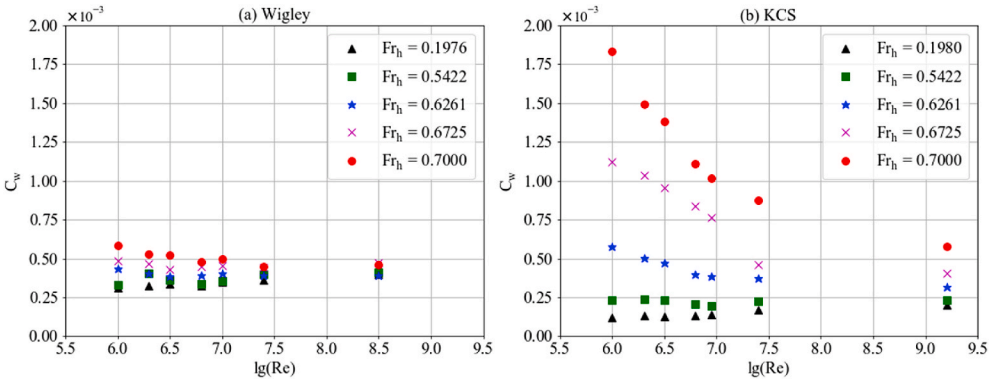

Fig. 7. Results of C_w of a) the Wigley hull, and b) the KCS, against lg(Re) with various depth Froude number (Fr_h).

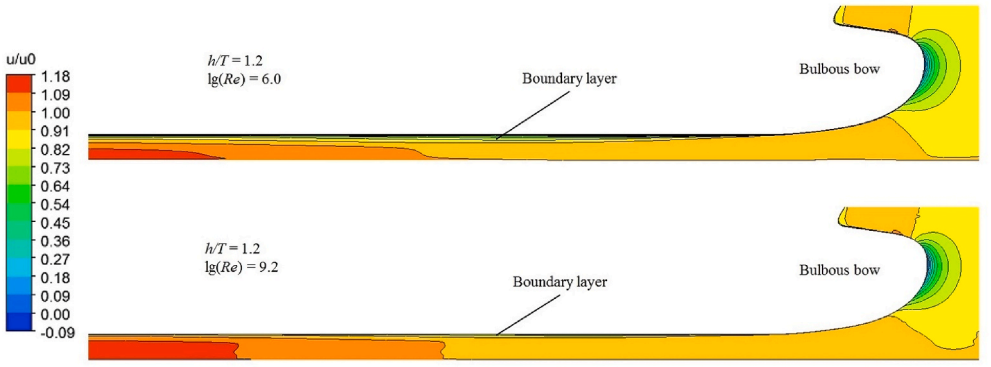

Fig. 8. Contours of velocity at $y = 0$ for part of the space under the KCS for lg(Re) = 6.0 (top) and lg(Re) = 9.2 (bottom) (u is flow velocity, u_0 is the incident flow velocity).

the efforts of conducting double-body computations can be saved.

In this study, ΔC_w (or ΔC_f) is defined by subtracting C_w (or C_f) in a shallow water case by C_w (or C_f) in the deep water case, at the same Re and Fr_h, i.e., ΔC_w (or ΔC_f) represents shallow water effects on the wave-making (or frictional) resistance coefficient. Based on the CFD results, ΔC_w plotted against ΔC_f for both the Wigley hull and the KCS are shown in Fig. 9.

For Wigley hull, the maximum ΔC_f is less than 3.0×10^{-4}, and the corresponding ΔC_w is about 3.0×10^{-4}. However, for the KCS, which is much fuller than the Wigley hull, the maximum ΔC_f is about 8.0×10^{-3}, and the corresponding ΔC_w reaches 15.0×10^{-4}, which is four times larger than in the Wigley case. This phenomenon reveals the ship form dependency of both ΔC_f and ΔC_w. Based on all the points in Fig. 9, a relation between ΔC_f and ΔC_w can be fitted with $R^2 = 0.96$ (coefficient of

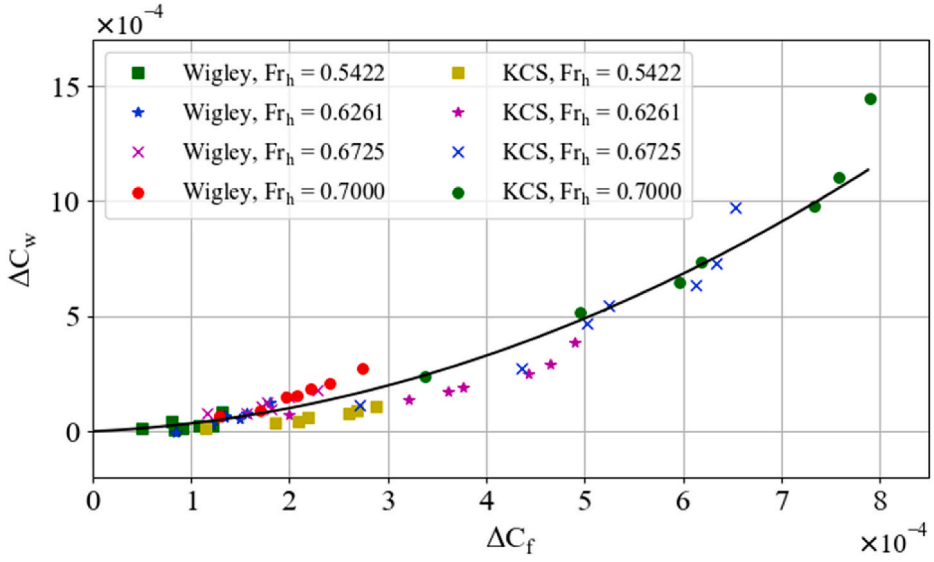

Fig. 9. Relation between ΔC_f and ΔC_w for both the Wigley hull and the KCS with various Fr_h (ΔC_w (or ΔC_f) is defined by subtracting C_w (or C_f) in a shallow water case by C_w (or C_f) in the deep water case, at the same Re and Fr_h).

determination) using MATLAB ($Fr_h \leq 0.7$):

$$\Delta C_w = 1596 \cdot (\Delta C_f)^2 + 0.183 \cdot \Delta C_f \quad (15)$$

Based on equation (15), if the frictional resistance of a ship increases due to shallow water effects, the wave resistance of this ship will also increase accordingly. This generally confirms the strong relationship between ΔC_f and ΔC_w, and the viscosity dependency of C_w in shallow water is also consolidated. It should be pointed out that the character h/T does not appear in equation (15) because shallow water effects have already been included in ΔC_f. Equation (15) is applicable for the Wigley hull and the KCS when $Fr_h \leq 0.7$, which is in line with the range implemented in this study.

Furthermore, based on Fig. 5 (right part), C_f derived from double-body computations shows minor differences compared to computations with free surface. Therefore, the increase of C_f due to shallow water effects provided by double-body computations can also be used to predict the scale effects on C_w, even though its physical basis is not as strong as equation (15). In this case, only double-body calculations are required, and computations with free surface, which demand more computing efforts, can be avoided.

Finally, a recommendation is given for resistance tests in shallow water: If the bank effects are at an acceptablely low level, the ship model should be as large as possible to reduce scale effects on the wave-making resistance. Particularly, for relatively full ships, which are more sensitive to limited water depth, the extrapolation of resistance to full scale should be reevaluated in shallow water cases.

5. Conclusions

In this study, the scale effects on the coefficient of wave-making resistance (C_w) in shallow water have been discussed for two distinct hull forms: the Wigley hull and the KCS. An approach for obtaining C_w separately is discussed based on CFD computations with and without free surface. After calculating C_w with different values of y^+, the effect of water depth on C_w is shown to be one order higher than the effect of y^+. Based on the results of C_w at different ship/model scales, several conclusions can be drawn as follows:

- The traditional assumption that the wave-making resistance coefficient is independent of ship/model scale is still valid for $Fr_h \leq 0.5422$ and all values of Fr_h for slender ships, like the Wigley hull;
- Scale effects are observed for a relatively full ship in shallow water, i.e., the conditions of the KCS at $0.5422 < Fr_h \leq 0.7000$. For these conditions, Reynolds number has a significant influence on C_w and the traditional extrapolation of resistance to full scale should be reconsidered;
- A strong relationship is found for the changes in the coefficient of frictional resistance (C_f) and the changes in C_w between model scale and full scale. This finding can help to save computing efforts, i.e., the alterations in C_f, which are easier to determine in numerical computations, can be applied to predict scale effects on C_w;
- In general, scale effects on C_w decrease with an increasing Reynolds number. If the bank and blockage effects are at an acceptably low level, the ship model should be as large as possible to reduce scale effects on wave-making resistance.

The hull form dependency of the scale effects on C_w is observed in this study, but detailed effects of ship parameters cannot be provided since only two ship forms are analysed. More ships with different dimensions and hull coefficients are required to provide more usable information, which is recommended for future research.

Declaration of competing interest

The authors declare that they have no known competing financial interests or personal relationships that could have appeared to influence the work reported in this paper.

CRediT authorship contribution statement

Qingsong Zeng: Conceptualization, Methodology, Software, Validation, Formal analysis, Investigation, Writing - original draft. **Robert Hekkenberg:** Methodology, Resources, Supervision, Writing - review & editing. **Cornel Thill:** Validation, Resources, Supervision, Writing - review & editing. **Hans Hopman:** Supervision, Writing - review & editing.

Acknowledgment

This work is financially supported by the China Scholarship Council (CSC), No.201506950009. The authors also appreciate the contribution of Cartesius (the Dutch national supercomputer) with pilot project No.17172, based on which most numerical computations in this study are realized.

References

Airy, G.B., 1841. Tides and waves. Encycl. Metrop. (1817–1845. Mix. Sci. 3.
ANSYS, 2017. ANSYS® Academic Research, Release 18.1 (Help System, Fluent Theory Guide).
ASME PTC Committee, 2009. Standard for verification and validation in computational Fluid dynamics and heat transfer: ASME V&V 20. Am. Soc. Mech. Eng. https://doi.org/10.1016/S0160-4120(97)89943-6.
Cumberbatch, E., 1965. Effects of viscosity on ship waves. J. Fluid Mech. 23, 471–479.
Eça, L., Hoekstra, M., 2014. A procedure for the estimation of the numerical uncertainty of CFD calculations based on grid refinement studies. J. Comput. Phys. 262, 104–130.
Eça, L., Hoekstra, M., 2008. The numerical friction line. J. Mar. Sci. Technol. 13, 328–345.
Ellingsen, S.Å., 2014. Ship waves in the presence of uniform vorticity. J. Fluid Mech. 742.
Gotman, A.S., 2002. Study of Michell's integral and influence of viscosity and ship hull form on wave resistance. Ocean. Eng. Int. 6, 74–115.
Havelock, T.H., 1908. The propagation of groups of waves in dispersive media, with application to waves on water produced by a travelling disturbance. Proc. R. Soc. Lond. - Ser. A Contain. Pap. a Math. Phys. Character 81, 398–430.
ITTC, 2017a. Resistance test-Recommended procedures and guidelines 7.5-02-02-01. In: Proceedings of the 28th International Towing Tank Conference (Wuxi, China).
ITTC, 2017b. Practical guidelines for ship CFD applications-recommended procedures and guidelines 7.5-03-02-03. In: Proceedings of the 28th International Towing Tank Conference.
ITTC, 1957. No title. In: 8th International Towing Tank Conference (Madrid, Spain).
Javanmardi, M., 2015. The Investigation of High Quality Surfing Waves Generated by a Moving Pressure Source. University of Tasmania.
Kajitani, H., Miyata, H., Ikehata, M., Tanaka, H., Adachi, H., Namimatsu, M., Ogiwara, S., 1983. The Summary of the Cooperative Experiment on Wigley Parabolic Model in Japan. TOKYO UNIV, JAPAN.
Katsui, T., Asai, H., Himeno, Y., Tahara, Y., 2005. The proposal of a new friction line. In: Fifth Osaka Colloquium on Advanced CFD Applications to Ship Flow and Hull Form Design (Osaka, Japan).
Kim, W.J., Van, S.H., Kim, D.H., 2001. Measurement of flows around modern commercial ship models. Exp. Fluid 31, 567–578.
Lamb, H., 1932. Hydrodynamics. Cambridge university press.
Li, Y., Ellingsen, S.Å., 2016. Ship waves on uniform shear current at finite depth: wave resistance and critical velocity. J. Fluid Mech. 791, 539–567.
Mucha, P., Deng, G., Gourlay, T., Moctar, E., Ould, B., 2016. Validation studies on numerical prediction of ship squat and resistance in shallow water. In: 4th MASHCON-International Conference on Ship Manoeuvring in Shallow and Confined Water with Special Focus on Ship Bottom Interaction, pp. 122–133.
Putnam, J.A., Johson, J.W., 1949. The dissipation of wave energy by bottom friction. Eos, Trans. Am. Geophys. Union 30, 67–74.
Raven, H.C., 1996. A Solution Method for the Nonlinear Ship Wave Resistance Problem. Doctor's Thesis. Delft Univ. Technol.
Raven, H.C., Van der Ploeg, A., Starke, A.R., Eça, L., 2008. Towards a CFD-based prediction of ship performance—progress in predicting full-scale resistance and scale effects. In: Proc. RINA-CFD-2008 (London, UK).
Sharma, S.D., 1963. A Comparison of the Calculated and Measured Free-wave Spectrum of an Inuid in Steady Motion. International Seminar on Theoretical Wave Resistance, Ann Arbor, Michigan.
Stern, F., 1986. Effects of waves on the boundary layer of a surface-piercing body. J. Sh. Res. 30, 256–274.
Terziev, M., Tezdogan, T., Oguz, E., Gourlay, T., Demirel, Y.K., Incecik, A., 2018. Numerical investigation of the behaviour and performance of ships advancing through restricted shallow waters. J. Fluid Struct. 76, 185–215.

Zeng, Q., 2019. A Method to Improve the Prediction of Ship Resistance in Shallow Water. Delft University of Technology.

Zeng, Q., Hekkenberg, R., Thill, C., 2019a. On the viscous resistance of ships sailing in shallow water. Ocean Eng. 190 https://doi.org/10.1016/j.oceaneng.2019.106434.

Zeng, Q., Thill, C., Hekkenberg, R., 2019b. Shallow water effects on ship-generated waves. In: 5th International Conference on Ship Manoeuvring in Shallow and Confined Water (MASHCON 2019) (Ostend, Belgium).